# Hybrid Network-Based Automatic Seamline Detection for Orthophoto Mosaicking

Wei Yuan, *Member, IEEE*, Yang Cai, and Jonathan Li, *Fellow, IEEE*

***Abstract*— Seamline detection is a crucial procedure for orthophoto mosaicking. To eliminate the seam effect caused by geometric discontinuities, seamlines must avoid crossing areas containing the obvious ground object, for which manual processing is usually required. Many existing seamline detection methods can generate seamlines bypassing most of the obvious ground objects but always take pixel-level computation, which may consume much time. To address this problem, this article presents a seamline detection approach based on a hybrid network search. First, without auxiliary data, the semi-global block matching (SGBM) algorithm was adopted to generate a disparity map for pairwise orthophoto overlapping area. By using adaptive threshold segmentation, a binary cost map containing the ground objects was obtained. Subsequently, a hybrid network was constructed by edge points and uniform points extracted on the cost map. Finally, seamlines were detected by search on this network-based graph. The essential contribution of the proposed method is that the seamline is searched on a sparse hybrid network instead of a raster cost map. Thus, computational complexity can be significantly decreased and produces fine-tuned seamlines. A series of comparison experiments were carried out between the proposed and well-established methods, using two benchmark datasets with different characteristics. The comparison results demonstrated that the proposed method could generate high-quality seamlines in terms of visual comparison and statistical evaluation. Moreover, the processing speed has a nearly tenfold improvement compared with the control group methods.**

***Index Terms*— Digital orthophoto map (DOM) mosaicking, disparity map, hybrid network, seamline.**

## I. Introduction

A TYPICAL problem for large-scale DOM mosaicking is geometry misalignment between adjacent orthophotos, leading to dislocations and fractures in final mosaicking. In orthoprocessing, the image is rectified by a digital evaluation model (DEM) instead of a digital surface model (DSM). This may cause a projection displacement when sharp height discontinuities occur, especially for the apparent object. When the seamline crosses through these areas, the mosaicking seam occurs. Therefore, to create a seamless mosaicked image, the criteria of optimal seamline detection are to avoid crossing the apparent ground objects.

Generally, the optimal seamline detection approaches contain two steps. The first step is constructing the cost map of the orthophoto overlaps. The typical cost commonly uses pixel-based features, such as gray difference, edge feature, and normalized correlation coefficient (NCC). The calculation of the pixel-based cost is fast but cannot detect objects completely. The second step is to search the seamline by optimizing the energy function according to the cost map. Many existing methods search seamlines on a raster-based cost map and perform cost minimization on a graph consisting of closely aligned pixels. The complexity of graph-based algorithms is an exponential function of the graph node numbers [1]. When the number of cost map pixel increases, the computation time increases exponentially. Therefore, the cost map is often calculated using a finite buffer or downsampling to reduce the size. In addition, heuristic strategies, such as A* and super pixel-based algorithms, are applied to reduce the computational overhead.

A raster cost map, densely packed with pixels, most pixel traverse operations can be saved in seamline search. Generally, a network-based graph requiring only a small number of nodes can serve as an efficient alternative to the raster cost map. In Fig. 1, the process of path finding from the starting point (orange nodes) to the endpoint (cyan nodes) involves navigating to avoid impassable areas (red nodes). In the left diagram, the search involves traversing through each accessible blue node. In contrast, the right diagram shows that the search is conducted directly on the yellow-marked network.

In this study, we ensure seamline accuracy by adopting a disparity map as a cost, allowing for the comprehensive detection of untraversable regions, such as buildings and trees. The disparity map serves as a robust tool, enabling the proposed method to outperform pixel-based cost methods and exhibit comparability with other object-based approaches. Instead of relying on a raster cost map, our approach conducts cost minimization on a hybrid network-based graph constructed from regular grid points and edge points extracted from a binary cost map. The utilization of this hybrid network enables precise determination of seamlines, bypassing projection displacement areas and maintaining regularity in vast traversable

Manuscript received 27 September 2023; revised 15 February 2024; accepted 20 April 2024. Date of publication 25 April 2024; date of current version 6 May 2024. This work was supported in part by the National Natural Science Foundation of China under Grant 41771479, in part by the National Plan for the Special Support of Leading Talents under Grant 412500002, and in part by the Japan Society for the Promotion of Science under Grant 23K13419 *(Corresponding authors: Yang Cai; Wei Yuan.)*

Wei Yuan is with the International Research Institute of Disaster Science, Tohoku University, Sendai 980-8572, Japan (e-mail: wei.yuan@tohoku.ac.jp).

Yang Cai is with Changjiang Spatial Information Technology Engineering Company Ltd., Wuhan 430010, China, and also with the School of Remote Sensing and Information Engineering, Wuhan University, Wuhan 430079, China (e-mail: Y.Tsai@whu.edu.cn).

Jonathan Li is with the Department of Geography and Environmental Management, University of Waterloo, Waterloo, ON N2L 3G1, Canada (e-mail: junli@uwaterloo.ca).

Digital Object Identifier 10.1109/TGRS.2024.3393626

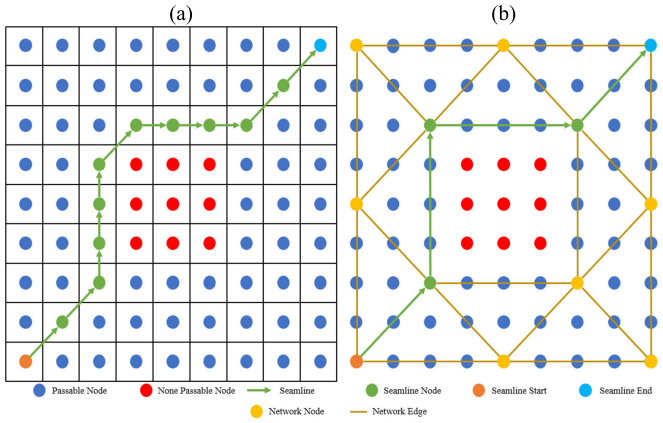


Fig. 1. Seamline search on the (a) grid and (b) network.

regions. Furthermore, the optimization process benefits from a substantial reduction in the number of nodes, accelerating the seamline search process. This article introduces a novel network-based graph search method, constructing a hybrid network based on seamline detection criteria. The network is simultaneously built using edge points extracted from the binary cost map and uniform grid points. It is characterized by a fine triangular network in narrow traversable areas and a regular grid in open traversable areas. Seamline search benefits from this design, allowing for fine bypassing in narrow traversable areas and maintaining a straight trajectory in open traversable areas.

This article is organized as follows. Section II provides an overview of related works. Section III presents the theory and implementation of hybrid network-based seamline detection proposed in this article. Section IV details the experimental setup and presents the results and analysis. Finally, Section V offers a comprehensive summary of the entire article.

## II. Related Works

Seamline detection methods have been widely studied. Pixel-based methods usually use the features of pixels to create a cost map and use a graph-based algorithm to find the minimal cost path as an optimal seamline. Kerschner [2] proposed a twin snake-based optimal seamline search algorithm. The algorithm uses color and texture similarity between images as a cost map; the initial twin snake is placed on the opposite side of the cost map; then, the snake model evolves until two snakes merge into one. Zhang et al. [3] proposed an ant colony-based seamline search method. First, the grayscale difference between images is computed as the cost constraint, and then, the ant colony algorithm is used to search for the optimal seamline. The computational cost of twin-snake and ant colony-based algorithms is high and potentially falls into a suboptimum path. Lin et al. [4] proposed an optimal seamline search algorithm by minimizing the maximum cost. The algorithm first uses an NCC to measure the cost and then iteratively increases the maximum difference value until the start and end points are connected. The iteration terminates, and the minimized maximum difference value is found. If the difference value of a pixel is greater than the maximum difference value, it is considered an untraversable region; if the difference value of a pixel is less than the maximum difference value, it is regarded as a traversable region. Finally, the algorithm uses Dijkstra's algorithm [5] to search for the shortest path from the starting point to the endpoint in the traversable region, i.e., the optimal seamline. Compared with the traditional Dijkstra shortest path search algorithm, the length of the seamline found by this algorithm is more extended, and fewer pixels in the untraversable region are crossed. Subsequently, Yuan and Zhong [6] improved the minimization maximum cost strategy by using the greedy algorithm for path selection, and this algorithm can find optimal seamline, but computational consumption is relatively high. Li et al. [7], [8], [9], [10], [11], [12] proposed an edge-enhanced seamline search method. The method first defines the cost function using traditional grayscale and gradient differences, then extracts and identifies the edges of obvious features, and enhances the energy map to constrain the mosaic lines better to bypass the obvious features, and high-precision seamlines can be obtained. However, the computation time is long due to the pixel-based graph-cut operation. Wang et al. [13] present a continuous space ant colony-based algorithm. The method first establishes a cost function based on gray differences and a gray gradient in the overlapping area. Then, a continuous space ant colony algorithm is established to select the minimum cost path for the optimal seamline iteratively. The pixel-based approach has the advantages of simple implementation and broad applicability, but the pixel features have discontinuity on the obvious features. Many buildings have smooth roof textures with little interpixel variability. Therefore, it is difficult for pixel-based methods to completely distinguish obvious features from other targets, which results in seamline crossing obvious features.

Auxiliary data-based methods usually utilize external data to constrain the seamline search, such as point cloud data, DSM, road and building vectors, and so on. Wan et al. [14] proposed an optimal seamline search method that combines road networks to ensure the seamline passes through the road area and avoids buildings. The method first superimposes the road network and the overlapping area to construct a weighted graph. It then uses the Floyd–Warshall algorithm [15] to find the shortest path on the weighted graph as the optimal seamline. Subsequently, Wang et al. [16] proposed an optimal seamline search method using a building vector map. This method first finds the centerlines between buildings and considers them as the initial seamlines. Since the building vector map is used, the initial seamline can avoid passing through buildings. The algorithm refines the initial seamlines using the area around to obtain the final seamline. In addition to the road and building vector maps, DSM is another commonly used auxiliary information Chen et al. [17] proposed an optimal seamline search method based on DSM. This method extracts DSM's elevation and finds the optimal seam line using Dijkstra's algorithm. The seamline can avoid crossing the obvious features by using the elevation information constraint. After that, various optimal seamline search methods based on DSM have been proposed [18], [19], [20], [21], [22]. In addition to the above auxiliary data, airborne point cloud

data are another frequently used auxiliary information. Ma and Sun [23] proposed an orthophoto mosaic based on point cloud data. This method uses airborne point cloud data to find all obvious features, set them as obstacles, and use the A* algorithm to optimize the optimal seam lines to avoid them. Methods based on auxiliary data are simple and efficient and can obtain high-quality seam lines. However, the disadvantage of such methods is that they require appropriate auxiliary information, which limits the usage scenarios.

Object-based methods usually utilize object-level features, such as image segmentation, disparity map, and semantic features to constrain the seamline search. Pan et al. [24], [25] proposed an optimal seamline search algorithm using image segmentation. The algorithm first uses a mean-drift algorithm to segment the overlapping area images, then calculates the change index of each segmented block, and then finds the traversable area using the minimization cost method. Finally, the algorithm optimizes the traversable area to obtain pixel-level seamline. Wang et al. [26] proposed a seamline search method using the watershed algorithm to segment the overlap images and measure the similarity between the segmented blocks and then also used the minimization of the maximum cost method to find seamline. However, for aerial images, segmentation based on mean drift or watershed algorithms is time-consuming, and the segmentation results are sometimes dissatisfactory due to the complexity of aerial image features. Disparity map is also commonly used to search for optimal seamline [27], [28]. This type of method first uses a semi-global matching (SGM) algorithm [29] to calculate the parallax map of the image in the overlapping region. The area with larger parallax is considered a prominent feature and removed, and the optimal seamline is searched in the remaining area. Li et al. [30] present a foreground segmentation-based method. This method segments the foreground region at the superpixel level as an untraversable area and is followed by pixel-level seamline optimization. Yuan et al. [31] used a D-LinkNet neural network to obtain a road probability map and used this map as a search constraint to guide seamlines through roads.

Most of the methods listed above focus on the innovative use of cost map, for seamline search generally uses a pixel-level graph search algorithm, which performs on the raster. Standard optimization methods include the snake model, ant colony algorithm, Dijkstra shortest path search algorithm, dynamic programming, graph cut, and so on. Different from these methods, this article proposes a method to search seamlines on a spare network build by edge point and uniform point, which can significantly reduce computational consumption and produce a regular line with fewer nodes.

## III. Method

The procedure of the proposed method can be mainly divided into two steps. Step 1 is the generation of the binary cost map. This step includes calculating the disparity map of the overlapped orthophotos and binary segmentation of the disparity map. Step 2 is the hybrid network searching. This step includes edge feature extraction, hybrid network construction, and optimal seamline searching. The process

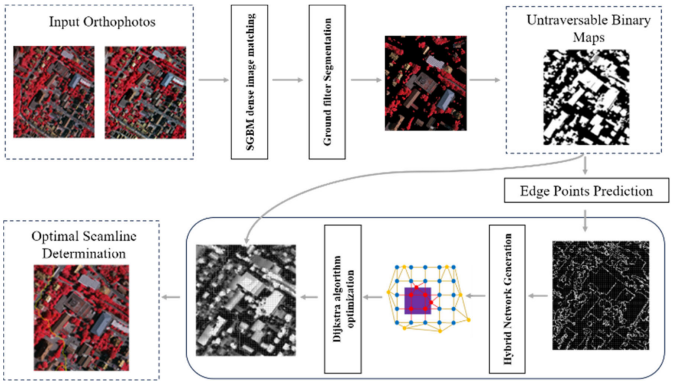


Fig. 2. Framework of the proposed method.

workflow of the proposed method is given in Fig. 2. The details of these specific principles and implementation processes are provided in Section III.

In orthophoto generation, the differential rectification is generally performed using DEM after filtering the ground features. Since the height information of surface features (e.g., buildings and bridges) is filtered, the projection displacements are not rectified correctly. Therefore, seamlines must avoid crossing this area. A disparity map can reflect the variation of feature heights; thus, this article used the disparity map to detect the projection difference region.

The semi-global block matching (SGBM) algorithm is used to calculate the disparity map. Instead of pixelwise global optimization, the SGMB uses dynamic planning only in a limited number of directions. Its energy function is as follows:

$$E(D) = \sum_{p} \left( \begin{array}{l} C\left(p, D_p\right) + \sum_{q \in N_p} P_1 T\left[\left|D_p - D_q\right| < 1\right] \\ + \sum_{q \in N_p} P_2 T\left[\left|D_p - D_q\right| > 1\right] \end{array} \right) \tag{1}$$

where $D$ represents the disparity map. $E(D)$ is the corresponding energy function for this disparity map. Here, $p$ and $q$ denote pixels in the image, and $N_p$ typically represents the eight-connected neighborhood of pixel $p$. $C(p, D_p)$ denotes the cost of the current pixel when its disparity is $D_p$. $P_1$ is a penalty term applicable to neighboring pixels of p, where the disparity values differ by 1. $P_2$ is another penalty term applicable to neighboring pixels of $p$, where the disparity values differ by more than 1.

The results of the SGBM calculation of overlapped orthophotos [see Fig. 3(a) and (b)] are shown in Fig. 3(c), which shows two adjacent orthophotos and the SGBM calculated disparity map. Fig. 3 shows that the disparity map can fully reflect the continuous height information of buildings, trees, and other higher features. It can provide a suitable seamline constraint as a cost map.

After obtaining the disparity map, a self-adaptive threshold segmentation method is employed to divide the parallax disparity map into binary regions, distinguishing traversable and untraversable areas. In real-world scenes, abrupt changes in height occur due to the presence of structures like houses and trees on the ground. Using a single threshold for segmentation yields less-than-ideal results in such scenarios. Therefore, this article introduces an adaptive moving threshold segmentation

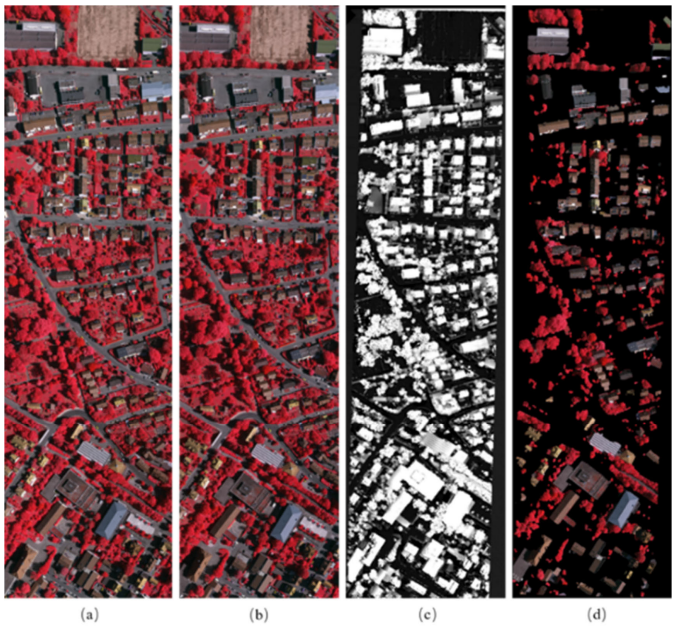


Fig. 3. Result of disparity map computation and adaptive binary segmentation. (a) Left orthophoto, (b) right orthophoto, (c) disparity map, and (d) binary segmentation map.

method to enhance the quality of segmentation results. The segmentation value for each pixel can be calculated

$$\text{result}\ (r, c) = \begin{cases} 255, & \text{if } D \text{ value } (r, c) > T(r, c) \\ 0, & \text{otherwise} \end{cases} \tag{2}$$

where $(r, c)$ is the computed gray value of the pixels in row $r$ and column $c$ on the binary cost map; the source $(r, c)$ is the gray value of the pixels in row $r$ and column $c$ on the source image. The threshold $T(r, c)$ is the average gray value of the $N^*N$ neighborhoods in the pixel $(r, c)$. This article chooses a smaller value $N$ set as 300 to ensure that obvious nonground objects can be segmented entirely. The segmentation results are shown in Fig. 3(d).

After the binary segmentation, the cost map is partitioned into traversable and untraversable regions, as illustrated in Fig. 4. In the binary segmentation map [see Fig. 4(b)], the raster delineates the traversable region (black) and the untraversable region (white). To validate the segmentation results, Fig. 4(a) utilizes the binary map to segment the orthophoto. It is evident that buildings and trees are completely separated, and the edges remain relatively intact. Therefore, based on the seamline detection criteria, this binary segmented map is deemed ideal for seamline constraint.

Seamline detection actually performs graph optimization on the cost map to find an optimal path that minimizes the cumulative cost. Then, widely used methods transfer it into graph-based search algorithms, such as Dijkstra, A*, ant colony algorithm, graph cut, Markov model, and so on. These kinds of search algorithms' time complexity were $O(En^2), n$ denotes the node numbers of the graph, and $E$ is the edge number of the graph. In practice, the image size is larger than $1000 \times 1000$, which means at least 1 million nodes in the search graph, it is already significant for computing.

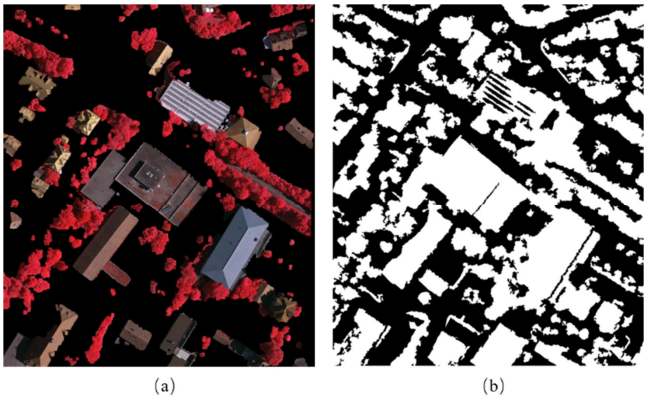


Fig. 4. (a) Binary mask segmented orthophoto. (b) Binary segmentation.

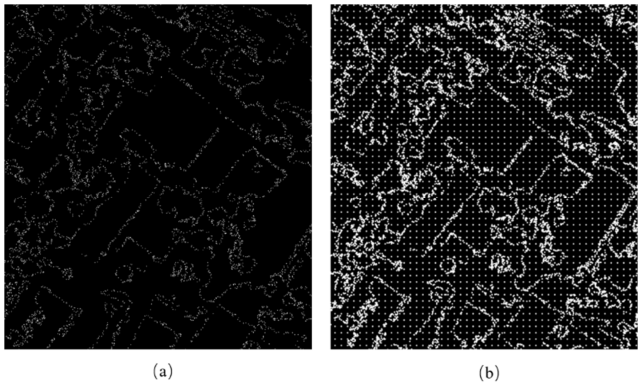


Fig. 5. (a) Edge point of untraversable region $P_{\text{edge}}$. (b) Mixture of $P_{\text{edge}}$ and $P_{\text{uniform}}$.

When image size increases $k$ times, the time complexity simultaneously $k^2$-fold magnifies.

### A. Hybrid Network Construction

In the binary cost map, traversable and untraversable regions are composed of numbers of pixels; consider them as nodes of a graph, where most nodes are redundant and do not need to be traversed.

Based on this idea, we proposed a hybrid network search method to substitute the traditional pixel-based search algorithm. First, edge extraction is performed on the obtained binary cost map. The point set obtained is the edges points of untraversable areas, recorded as $P_{\text{edge}}$. Then, uniformly distributed points with interval $n$ pixel on the cost map are calculated and recorded as $P_{\text{uniform}}$, and finally, mix $P_{\text{edge}}$ and $P_{\text{uniform}}$ as a new set of points recorded as $P_{\text{hybrid}}$. It can be seen in Fig. 5(a) that all the edge points of the buildings in the binary cost map are extracted, and Fig. 5(b) adds uniform grid points on top of this.

After $P_{\text{hybrid}}$ is obtained, use it as the initial seed point set of the Voronoi diagram algorithm to construct the hybrid network. To keep the edges of the network in the passable zone and simplify the network, the network edges on the untraversable region can be filtered

$$\text{Edge}(v_1, v_2) = \begin{cases} \text{deleted}, & \text{if cost}(v_1) \text{ or cost}(v_2) = 255 \\ \text{preserve}, & \text{if cost}(v_1) \text{ and cost}(v_2) = 0 \end{cases} \tag{3}$$

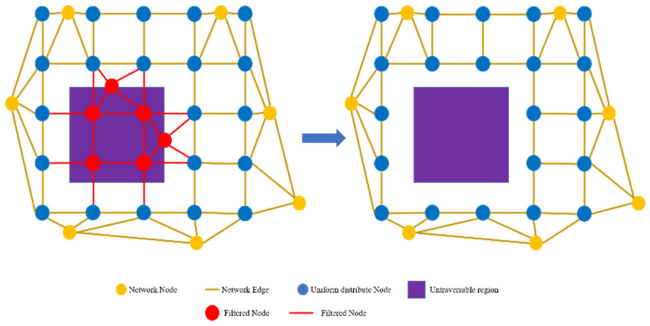


Fig. 6. Illustration of edge filtering in the hybrid network.

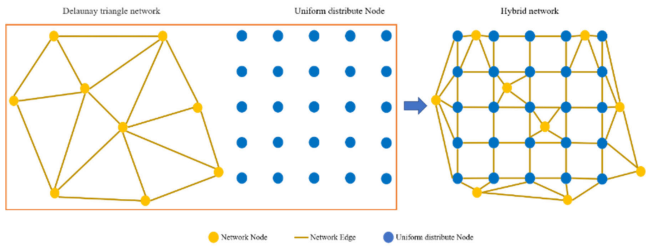


Fig. 7. Illustration of the Delaunay triangle network transformed into a hybrid network.

where Edge is the edge in the hybrid network. Each edge has two nodes; $v_1$ and $v_2$ are the edge nodes with coordinates $(r_1, c_1)$ and $(r_2, c_2)$ on the cost map. When any of the two nodes has a value of 255 on the binary cost map, this edge in the network is deleted. Only those edges where two nodes have a value of 0 on the binary cost map are preserved. As shown in Fig. 6, the purple square represents the untraversable region; all nodes are detected and marked as red if they fall into the untraversable region, i.e., the pixel value is 255 on the binary map. All edges associated with the filtered node are also marked red and finally deleted. When all edges matching the deletion criteria are filtered, the retained edges in the network are within the traversable region.

The major feature of the hybrid network is the inclusion of uniformly distributed grid points in the construction, and this brings a change in the geometry of the network from which seamline search can benefit.

Fig. 7 shows the geometry transformation of the corresponding Delaunay network constructed by $P_{\text{edge}}$ into a hybrid Delaunay network. Within the addition of $P_{\text{uniform}}$, regular nodes are added to the gaps of the $P_{\text{edge}}$ and linked up by edges. The Delaunay network has been reconstructed into a hybrid network. The same properties are retained when converting to Voronoi diagrams. It can be seen that the distribution of points determines the geometry of the network. In the network constructed by $P_{\text{edge}}$, the geometry is irregular and edges length are uneven, while the hybrid network maintains a regular geometry overall, nodes are connected by shorter and length-balanced edges.

As shown in Fig. 8, the Voronoi network constructed by $P_{\text{edge}}$ and hybrid networks constructed by $P_{\text{hybrid}}$ is overlayed on the binary cost map. Both networks are guaranteed that all the edges are on the traversable region. This can guide seamline go through traversable areas. In optimal

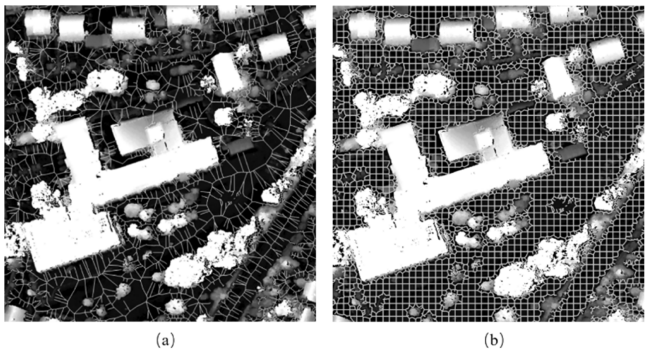


Fig. 8. Actual effect of (a) original Voronoi triangle network and (b) hybrid network on a cost map.

seamline detection, rather than a raster cost map represented by closely aligned pixels, only a small number of nodes need to be considered on this network. In practice, when the cost map size is 3000 × 10 000, the corresponding hybrid network node number is around 20 000, approximately reducing node number by 1000 times. Moreover, the hybrid network in Fig. 8(b) fills the large traversable area with a sparse grid and the smaller traversable area with a delicate triangle. Compared to the Voronoi network constructed by $P_{\text{edge}}$ in Fig. 8(a), the edge distribution of the hybrid network is more appropriate, ensuring both regularities in open space and fineness in narrow space. This brings great help for the subsequent seamline search.

### B. Hybrid Network-Based Seamline Search

After the hybrid network is constructed, seamlines will be searched on this network. The seamline search can be transformed into a least-cost path search. The optimal path search problems are generally solved using graph optimization.

The network can be regarded as a graph $G(E, V)$, where $V$ is the vertex of the graph and $E$ is the graph's edge. The seamline search searches for the path with the lowest cumulative cost in graph $G(E, V)$. With the benefit of significant node number reduction of the hybrid network, the greedy algorithm with no further heuristic strategy is appropriate for optimal seamline search.

This article uses Dijkstra's algorithm to search the optimal path for graph $G(E, V)$. The algorithm finds the optimal path by minimizing the cumulative edge weights on the path, and the weight of each edge is calculated by two endpoints. The original Dijkstra is used to search for the shortest path, and the cost of edges is set to the distance between two end nodes.

In order to make the algorithm suitable for hybrid network-based seamline search, in this article, the weight of the graph edge is redesigned according to the features of the cost map and the seamline generation criteria.

Since the entire network is on the traversable region, the obvious object with a certain elevation on the ground can be disregarded in the hybrid network. However, the binary segmentation only divided traversable and untraversable by threshold. When the height of objects in the area is uneven, some lower objects can be misclassification as the traversable region. Therefore, the node value on the disparity map is

TABLE I
DATASET DESCRIPTION

| Datasets | Image size (pixels) | Number of images | Spectators | GSD (m) | Area description |
|---|---|---|---|---|---|
| Vaihingen | 7680×13824 | 14 | IR-R-G | 0.1 | Rural |
| Katowice | 6296×4129 | 32 | R-G-B | 0.2 | City |

considered one of the edge weight items. Additionally, the seamline needs to be shortened in length and close to the centerline of the overlap region. Thus, the Euclidean distance between the node is also used as weighted terms of the edge. Edge weight is calculated by

$$W_{\text{edge}}(v_1, v_2) = \text{dist}(v_1, v_2) + (I_{r_1,c_1} + I_{r_2,c_2}) * 0.25 \quad (4)$$

$$\text{dist}(v_1, v_2) = \sqrt{(r_1 - r_2)^2 + (c_1 - c_2)^2} \quad (5)$$

where $W_{\text{edge}}$ is the weight of the edge, $v_1$ and $v_1$ are the two endpoints of the edge, which the coordinates are $(r_1, c_1)$ and $(r_2, c_2)$, respectively, and dist() is the Euclidean distance calculation function. Let $I$ denote the pixel value in the disparity map, where $I_{ij}$ represents the pixel value at coordinate $(i, j)$. After the weights of the edges in graph $G(E, V)$ are determined, the cost function of the seamline search is determined by

$$\text{Cost}_{\text{path}} = \sum_{v_i, v_j \in \text{path}} \text{Weight}(E_{ij}) \quad (6)$$

where $\text{Weight}(E_{ij})$ is the cumulative edge weights of Edge$(v_i, v_j)$. The optimal seamline search is to find the minimal cost path on graph $G(E, V)$.

After the start and end points of the seamline are determined, the Dijkstra algorithm is used to calculate the cumulative cost of each node in the $G(E, V)$ to the start point, and the path with the most minor cumulative cost is selected as the optimal seamline. Fig. 9(a) shows the hybrid network-based seamline search results overlaid with the disparity map. It can be seen that seamline is travel along the edges of the hybrid network, and lines are located in the region of the disparity map with values close to 0. Meanwhile, the hybrid network-based seamline results are shown in Fig. 9(b) overlaid with the corresponding orthophoto, and it can be seen that the seamline bypasses all the buildings and even avoids the trees with a certain height.

The hybrid network-based seamline search method can considerably reduce the number of nodes in graph search and result in fine seamlines to bypass the obvious ground features. More experiments are given in Section IV to illustrate the effectiveness of this method.

## IV. EXPERIMENT AND EVALUATION

### A. Design of Experiments

Two sets of comparison experiments were conducted to verify the algorithm's effectiveness in this article. They are using two open aerial orthophoto datasets provided by the ISPRS society. The details of the two datasets are listed in Table I.

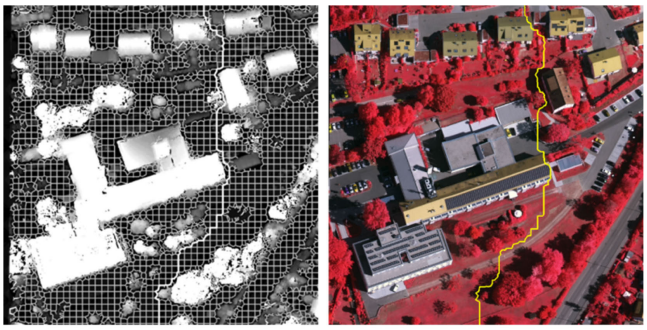

(a) (b)

Fig. 9. Optimal seamline searched on the hybrid network. (a) Overlay on the network and (b) overlay on orthophoto.

The comparison experiments have five groups: 1) the edge Voronoi-based seamline search method [32], 2) the foregrounds segmentation-based method, abbreviation FGS-based method [33], 3) commercial software OrthoVista, 4) a seamline algorithm proposed by Song et al. [34], and 5) jump point search (JPS)-based method [22].

The first group in the edge Voronoi-based method uses the same disparity cost map as the hybrid-based method. The key distinction lies in the hybrid network-based method's use of both edge points and uniformly distributed points during network construction, while the edge Voronoi-based method exclusively relies on edge points. This group aims to validate the benefits of regularity in seamline search introduced by the hybrid network. The second group employs the superpixel segmentation algorithm to calculate the foreground as the untraversable region. It utilizes graph cut to determine the superpixel optimal buffer, ultimately computing the pixel-level optimal seamline on the superpixel buffer. This group assesses the efficiency of the hybrid network-based method compared to the heuristic pixel-based search method. Despite both approaches utilizing object-level cost, a similar level of accuracy is expected. In the third group of experiments conducted by OrthoVista, we adopted a method proposed by Song in the fourth set. This involves refining the seam lines through marker-controlled watershed segmentation in dilated EMPs, with CUDA optimization significantly enhancing efficiency at the implementation level. The fifth experimental set employed a fast seamline detection method based on JPS. This approach substantially improved efficiency and reduced resource consumption by bypassing the evaluation of numerous image pixels. Results from each experimental group will be quantitatively evaluated for accuracy and efficiency, using the number

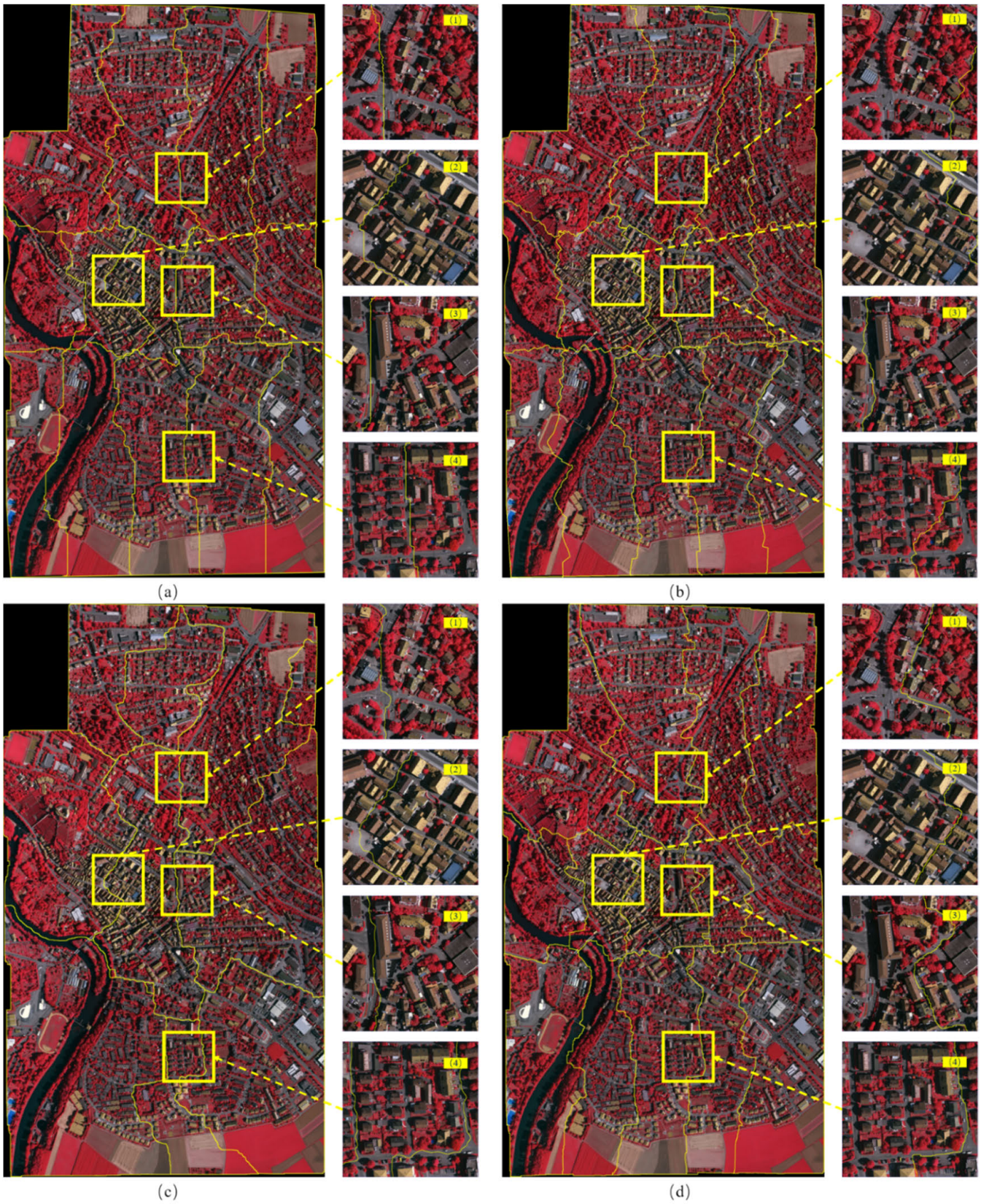


Fig. 10. Results obtained on Vaihingen dataset using (a) proposed method, (b) edge Voronoi-based method, (c) OrthoVista software, and (d) FGS-based method.

of traversed buildings for accuracy and the total operating time for efficiency.

The proposed algorithm is developed using C++ in the visual studio 2022 environment, applying OpenCV 4.5.0 and boost1.76. The test machine was a 3.20-GHz Intel Core i7-10750H CPU with 16-GB RAM running Windows 10. Additionally, the interval of uniformly points $n$ was configured as 8.

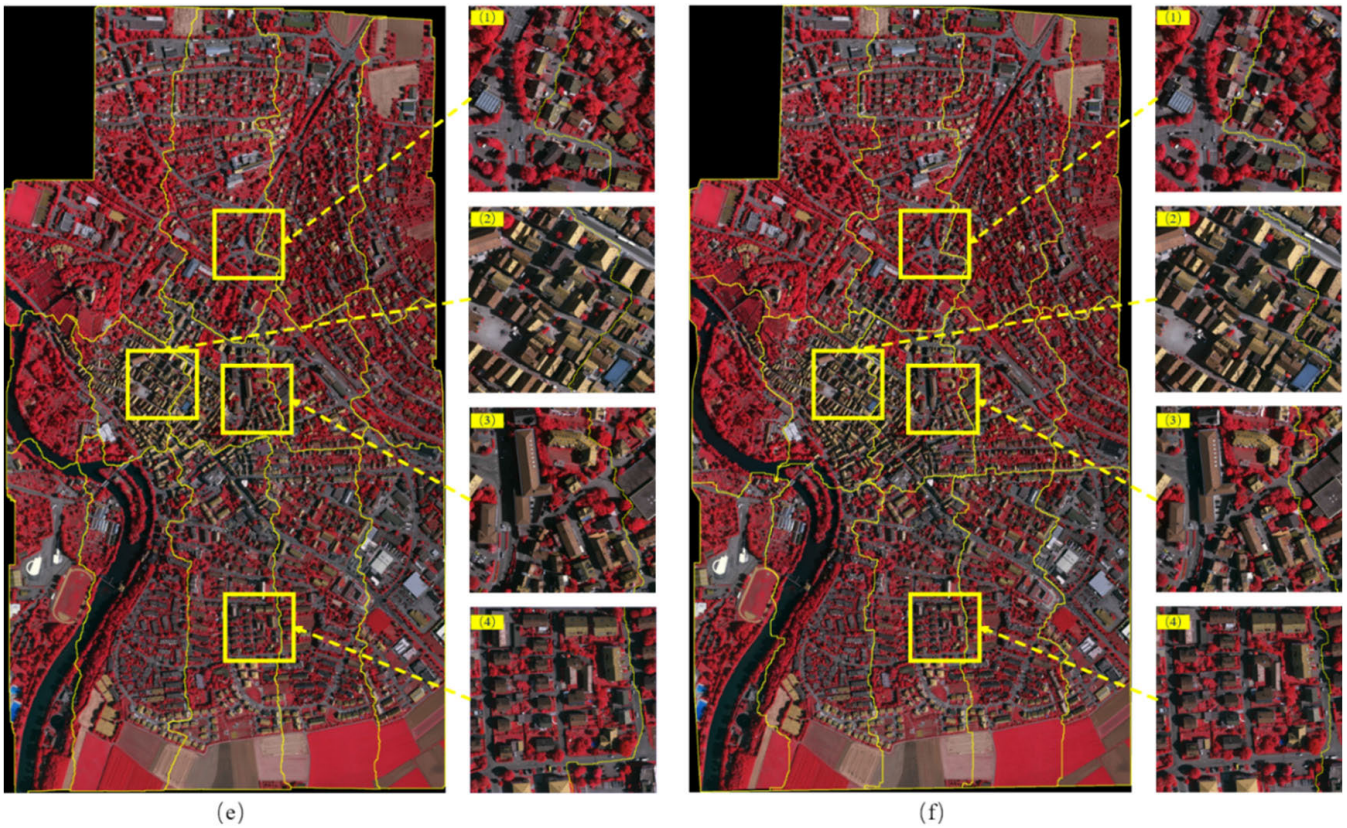


Fig. 10. *(Continued.)* Results obtained on Vaihingen dataset using (e) Song's method and (f) JPS-based method.

### *B. Result*

The experimental results of seamline detection for the first Vaihingen dataset are shown in Fig. 10. All six sets of algorithms compute the optimal seamline network. Each set of experiments shows the overview of the seamline network and six selected partial zoom views to demonstrate the result in detail.

From the overview, the proposed methods achieved the most regular seamline network among the six sets of results; in the traversable zone, the proposed algorithm searches for straight seamlines and only performs precise avoidance in the untraversable zone, stemming from its inclusion of regular grid nodes, which significantly benefits the overall seamline regularity. Other methods may not exhibit the same regularity as the proposed method. All the methods maintain a well-defined network framework and circumvent large building areas.

In terms of details, in the first set of enlarged views, both the proposed method and the OrthoVista software choose to pass through the road, on the basis of which the proposed method also maintains a straight line through. The edge Voronoi-based, FGS-based, Song's, and JPS-based methods [see Fig. 10(b)(1), (d)(1), (e)(1), and (f)(1)] choose to pass between separate buildings. The second set of enlarged views is a dense building scene, where the proposed algorithm in Fig. 10(a)(2) and OrthoVista in Fig. 10(c)(2) choose a more reasonable path on the widest gap between dense buildings. The FGS-based, Song's, and JPS-based methods [see Fig. 10(d)(1), (e)(1), and (f)(1)] also bypass the buildings but through a narrower traversable zone. However, the edge Voronoi-based method in Fig. 10(b)(2) crosses through the buildings in this scene which is negative. In the third view, the first three sets of seamlines pass through the traversable road [see Fig. 10(d)(1), (e)(2), and (f)(3)]. In contrast, the FGS-based, Song's, and JPS-based methods pass through the narrow building gap [see Fig. 10(d)(3), (e)(3), and (f)(3)], but the seamline is longer. The fourth enlarged view scene is low buildings with large gaps, and all six groups of methods go through the passable gap area. In Fig. 10(a)(4), the proposed method still achieves the best visual effect, presenting a straight line.

The visual results from four enlarged views indicate that all methods can effectively guide seamlines to circumvent impassable areas. Notably, the proposed method stands out with its superior line regularity and straight paths in traversable areas. Additionally, when selecting paths for seamline traversal, our approach prioritizes larger traversable areas, such as roads and open spaces. In contrast, other methods' seamlines often navigate through narrow gaps between buildings. Consequently, in the final mosaic results, will have a distinct advantage.

The accuracy and efficiency of the six groups of methods have been evaluated; the statistical results are shown in Table II.

The number of buildings crossed indicates the accuracy of the seamline generation. Statistically, FGS achieved the best results, with just seven crossings in the whole area, and the proposed method also achieved good results, with nine crossings. In general, the methods based on object-level

TABLE II
RESULTS OBTAINED FROM THE TWO DATASETS

| Method | Number of building crossed | | Process time (s) | |
|---|---|---|---|---|
| | Vaihingen | Katowice | Vaihingen | Katowice |
| Ours | 9 | 7 | 47 | 38 |
| Edge Voronoi-based | 10 | 15 | 41 | 33 |
| OrthoVista | 15 | 47 | 1033 | 718 |
| FGS-based | 7 | 4 | 631 | 477 |
| Song's method | 33 | 56 | 73 | 62 |
| JPS-based method | 11 | 13 | 53 | 44 |

cost maps are cross less obvious building. In contrast, OrthoVista and Song's method, due to its possible use of a pixel-level cost map, is unsatisfactory in terms of accuracy, with 15/33 crossings. Regarding processing time, the network search-based algorithm reduces the computation time by almost ten times compared to the FGS-based method and OrthoVista. This is because the number of nodes traversed by the network search is significantly lower than the pixel-based search. Additionally, Song's method achieves notable speed due to extensive CUDA optimization at the implementation level. However, its efficiency still falls short compared to our approach. The JPS-based method demonstrates efficiency comparable to our method, due to its effective JPS algorithm. However, as this search algorithm is suboptimal, the method traverses more buildings than ours.

The second group of the Katowice area is a typical urban area. Unlike the low detached buildings in the previous dataset, the buildings in this dataset are taller and very dense, making the generation of seam lines more complex. Fig. 11 shows the seamline results obtained using the six methods.

All the methods generated seamline networks that successfully navigated bypass dense buildings area. However, OrthoVista's mosaic area is very uneven in size, and the distance between the lines is too close or even overlapping. The proposed method still has an advantage in the seamline network's regularity, which is more evident in the suburbs of the scene where there is a sizable passable area, and lines are oriented close to horizontal or vertical. In inner-city scenes where the traversable area is narrow, there are also fewer twists and turns in seamlines compared to other methods.

In the first set of enlarged views, FGS in Fig. 11(d)(1) works best where the seamline is farthest from the buildings; the remaining three methods are closer. In Fig. 11(a)(1), the proposed method crosses the buildings on a small part; it is attributed to SGBM being relatively ineffective in the vertical direction, and there are some incomplete extractions of the untraversable zone. The second set of enlarged views shows that most of the methods create seamline avoided the untraversable areas, except for OrthoVista and JPS-based method [see Fig. 11(c)(2) and (f)(2)], which crosses a large circular building resembling sports arenas. Moreover, the proposed method has a more reasonable choice of the shorter path due to its use of the distance term in the energy function. The third group is a typical urban area with dense, tall buildings; the only passable areas are the narrow roads between buildings. The seamline of the proposed method in Fig. 11(a)(3) and the FGS-based method in Fig. 11(d)(3) can pass from the road precisely. Song's method and JPS-based method are performed poorly in this scene [see Fig. 11(e)(3) and 11(f)(3)]. Furthermore, in Fig. 11(b)(3), the edge Voronoi method has a seamline search that ultimately failed in this scene because the network-based search method may break into several small subgraphs when the impassable area obscures too extensive a range. The proposed method solves this problem by incorporating regular grid points. The fourth scene is also a tall building block, but its adequate space is relatively more significant, and none of the methods cross through any obvious buildings. Visually, the proposed method has the advantage of a more concise and clean line. The FGS method is more refined and avoids all the cars on the road, which stems from its advantage in pixel-level search.

From the visual results of this dataset, it can be concluded that the pixel-level cost-based method (e.g., OrthoVista and Song's method) exhibits shortcomings in handling large monolithic buildings, often leading to incomplete extraction and seamlines crossing such structures. Furthermore, the vertical alignment direction of the images in this dataset has a certain impact on the integrity of the SGBM parallax algorithm. The network-based algorithm, due to its high simplification of the cost map, struggles when the impassable zone is too extensive, hindering effective seamline searches. The statistical results of second dataset are also given in Table II.

Benefiting from the pixel-level search, the FGS-based method remains the best in the accuracy metrics, with only four buildings crossed. The proposed method maintains good single-digit results due to the adopted object-level cost map. The JPS and edge Voronoi-based method lags significantly behind the first two methods in this metric, reaching 13/15 traversals. OrthoVista remains the last to traverse 47 buildings in this metric. Song's method performed the worst which have 56 crosses, primarily because it utilized a simplistic pixel-level cost map. Network-based search methods have a considerable advantage in the process time metrics. The proposed method consumes 5 s more than the edge Voronoi-based method due to the introduction of regular grid points, which increases the number of nodes in the graph search. Pixel-level search-based like FGS-based method and OrthoVista, the time consumption is much higher. Since FGS uses a superpixel-based heuristic strategy, it still has an advantage in processing time over OrthoVista. Song's and JPS-based methods exhibit efficiency comparable to network-based search methods.

The visual effect and statistical result of the above experiments show that the proposed method is better than the pixel-based cost method in terms of accuracy and equal to the object-based cost method. Moreover, the efficiency of the proposed method is significantly better than the pixel-based search method; in addition, the proposed method generates seamlines with more regularity, less distortion, and less cornering.

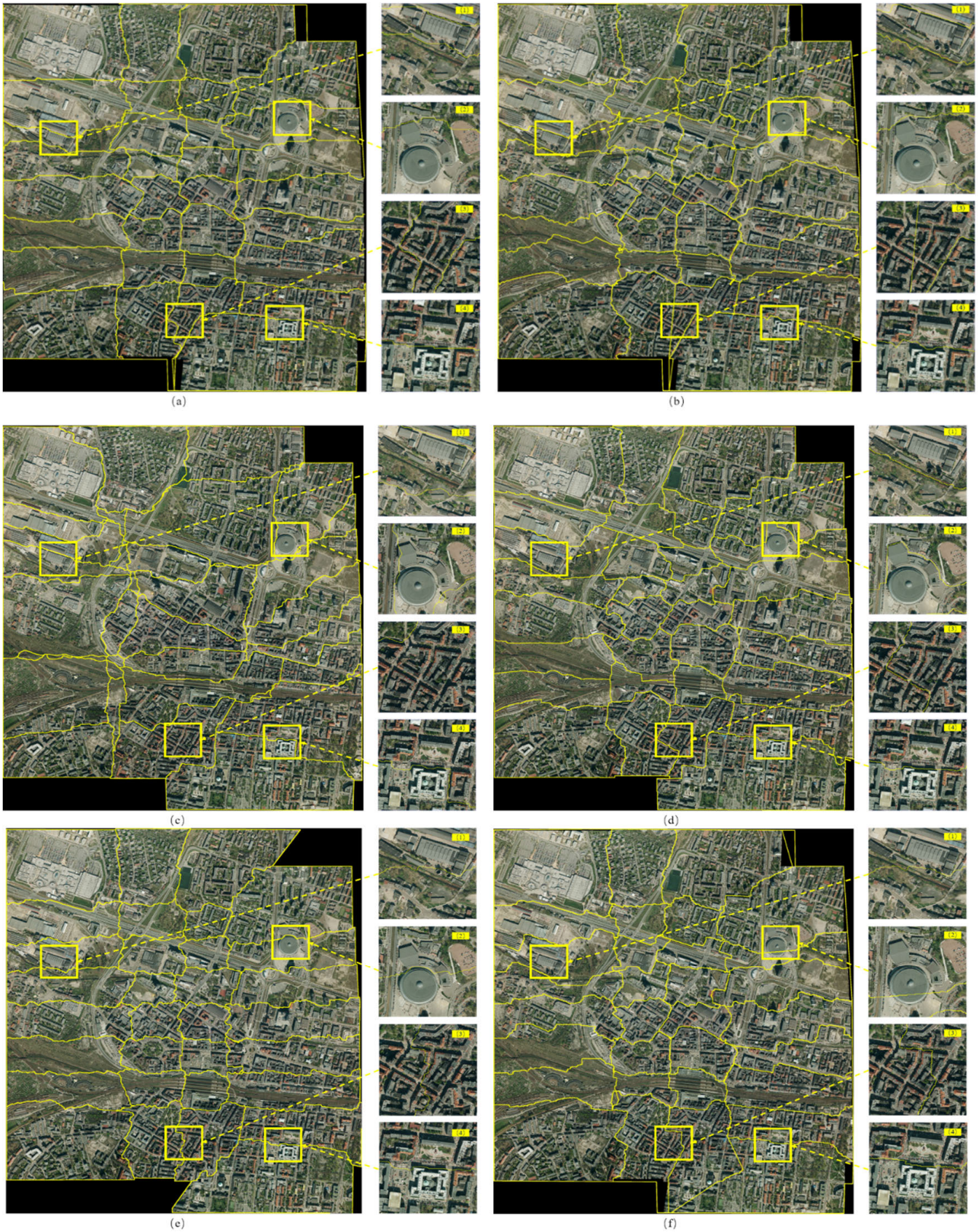


Fig. 11. Results obtained from Katowice dataset using (a) proposed method, (b) edge Voronoi-based method, (c) OrthoVista software, and (d) FGS-based method, (e) Song's method, and (f) JPS-based method.

TABLE III
TRAVERSAL NODE REDUCTION IN TWO DATASETS

| Method | No. of graph nodes | | Corresponding raster size (pixels) | | Traversal node reduction (%) | |
|---|---|---|---|---|---|---|
| | Vaihingen | Katowice | Vaihingen | Katowice | Vaihingen | Katowice |
| Ours | 18211 | 13242 | 3321×5731 | 2651×3192 | 99.91 | 99.84 |
| Edge Voronoi-based | 16723 | 12424 | | | 99.91 | 99.85* |

* The values in Table 3 are statistical averages of each two overlapping regions, which are calculated by dividing the total number by the number of overlapping regions

The criteria of optimal seamline detection are avoiding obvious ground objects. During detection, the quality of the cost map is the most significant impact on accuracy. Pixel-level cost-based methods, such as OrthoVista and Song's methods, traversed more buildings in two dataset trials due to the inability of pixel level cost map to maintain the integrity detecting result. The rest method utilizes object-level cost map, achieving better results. It is also worth mentioning that the proposed algorithm uses a binary cost map model. Although the adaptive threshold segmentation is used, there will be missed detection if the height of buildings in a region varies too much. The FGS-based method also suffers from this problem, and the segmentation results vary greatly when parameters are chosen differently.

The proposed method's most significant advantage lies in the network construction on passable regions, leading to a reduction in traversed nodes in two key aspects. First, through binarization of the disparity map, the regions are categorized into passable and nonpassable, resulting in the removal of network edges on nonpassable regions along with the associated nodes. Second, a Voronoi triangular network is established within the traversable area. This raster cost map, represented by closely spaced pixels, is effectively captured by a network containing only a limited number of nodes and connected edges.

According to Section III, all optimal seamline search methods can be categorized as graph optimization. The computational time complexity of graph optimization methods is $O(En^2)$, which is a function of edge $E$ and node $V$ in $G(E, V)$ ($n$ is the number of node $V$), while the number of nodes is a quadratic term. The vast majority of methods deal with the raster cost map as a graph; if the network-based method reduces the nodes number to 0.1 of the original, then the computational complexity is reduced by 0.01. In Table III, the average node numbers of the graph searched by the proposed method and the edge Voronoi-based method in two sets of experiments are processed by statistically, and the corresponding raster cost map size is also shown in Table III.

Both methods reduce the graph nodes in the overlap region to one thousandth. However, the experimental time consumption statistics in the previous section do not achieve such a high speedup ratio due to the high computational consumption of the disparity map computing. In addition, the special generation rules of the network limit the computational speed. Regardless of the above, the network-based search method has achieved a nearly tenfold improvement in time consumption compared to FGS-based method and OrthoVista. It is worth noting that although the proposed method adds regular grid points, the average number of nodes does not increase significantly compared to the edge Voronoi-based method, so the final calculation time does not increase significantly either.

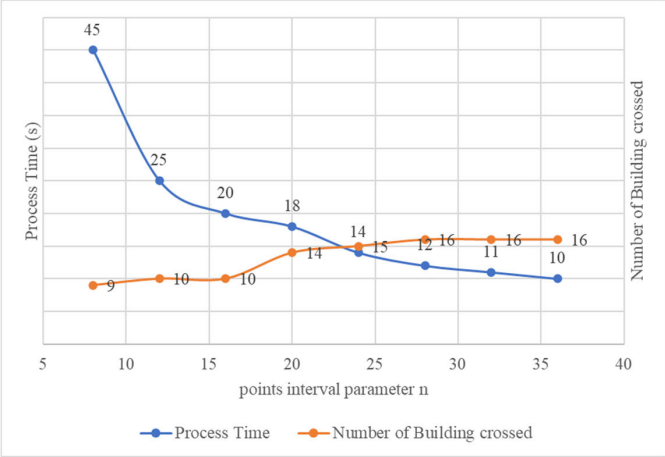


Fig. 12. Effect of points interval $n$ on algorithm efficiency and seamline quality in Vaihingen dataset.

To better illustrate the relationship between the number of vertices in the network, algorithm efficiency, and seamline quality, we conducted several sets of experiments using our proposed method in the Vaihingen dataset. In these experiments, the parameter n for uniformly distributed points interval was varied, and corresponding curves were plotted in Fig. 12.

The interval $n$ was set to a series of values ranging from 8 to 36 with a step size of 4. From the graph, it can be observed that as n increases, the processing time decreases while the number of buildings crossed increases. This is attributed to the decrease in the total number of points in the hybrid network as fewer uniformly distributed points are added when n increases, leading to faster computations. Additionally, with the increase in $n$, the points in the traversable regions of the network decrease, potentially causing the algorithm to miss some optimal paths, resulting in seamlines crossing smaller buildings. Additionally, as $n$ increases, the trends of the two curves tend to flatten out.

The primary distinction between the proposed method and existing approaches lies in the direct execution of the search on the hybrid network. Additionally, the proposed hybrid network

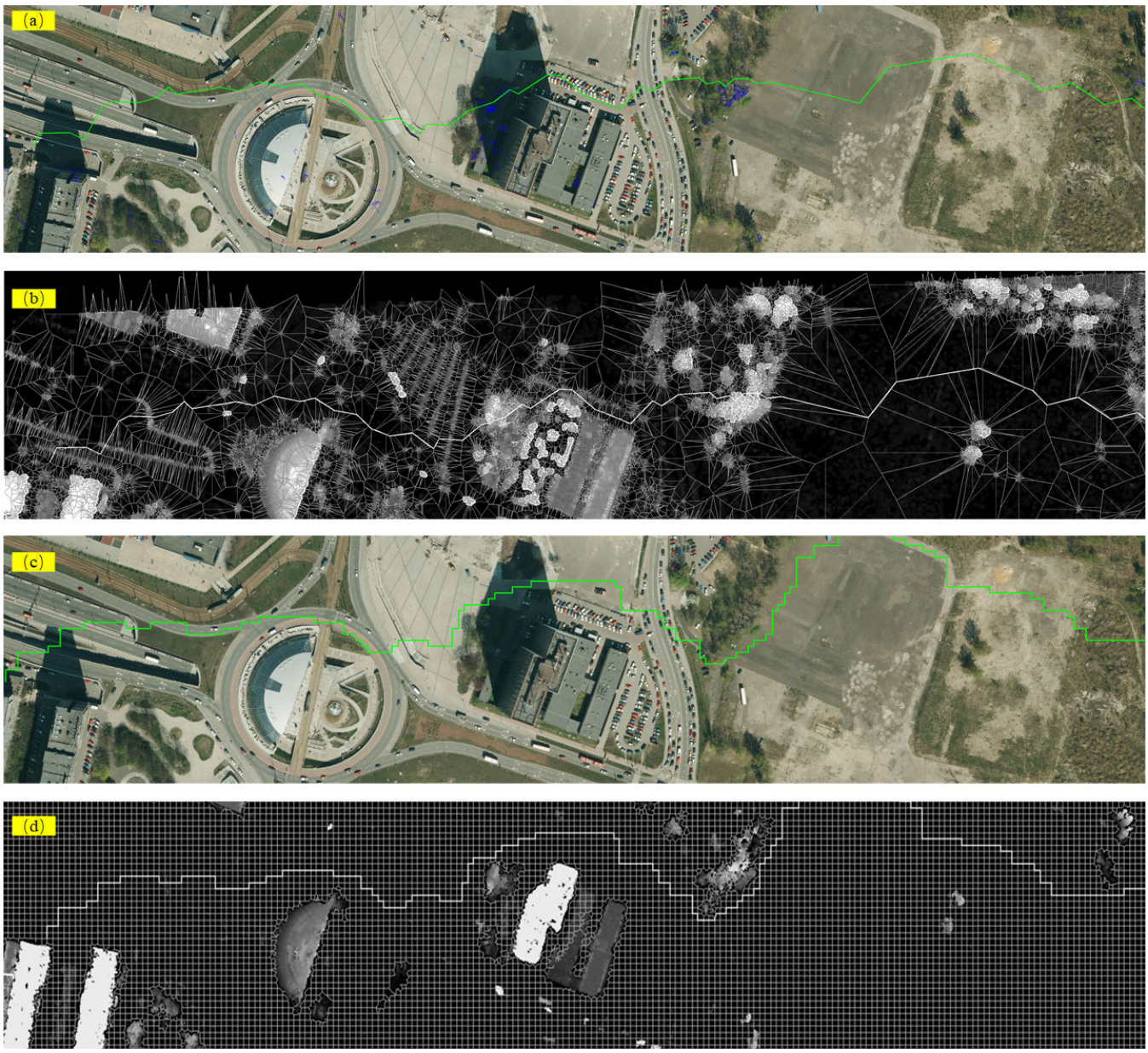


Fig. 13. Local enlarged view of the seamline results overlay on orthophoto and the corresponding network (a) and (b) generated using edge Voronoi-based method and (c) and (d) using our method, respectively, which were obtained from Katowice dataset.

holds a notable advantage over the edge Voronoi network. The seamline results in the Katowice dataset, as depicted in Fig. 13, reveal that both the edge Voronoi-based method and the proposed hybrid network can effectively navigate around prominent buildings. However, a noticeable difference emerges when examining the superimposed network diagrams. In the edge Voronoi-based method, the network edges are generated on the vertical bisector of the edge points in the untraversable zone, aligning the seamline orientation with the centerline between buildings. Yet, uneven distribution of buildings leads to varying edge point densities. This causes irregularities in the seam lines, creating strange angles, especially in sparse areas, as depicted in Fig. 13(b). In contrast, the proposed hybrid network utilizes both building edge points and regular grid points as seed points. This approach offers two advantages: first, in the dense building areas, the network edges align with the centerline, ensuring seamline passage through narrow areas; and second, in the open areas, the edges generated by regular points form strict grids, maintaining seamline regularity. Notably, regular grid points primarily affect the network at widths exceeding the grid distance, while building edge points contribute to network construction in narrow passable areas, where the traversable width is less than the grid distance. In essence, the hybrid network achieves precision in narrow spaces and regularity in wider areas. As shown in Fig. 13(d), the seamline follows fine network edges in narrow passable zones and adheres to regular lattice edges in wider passable zones. Comparing Fig. 13(a) and (c), the edge Voronoi-based mosaic line bypasses obvious features but exhibits a curved direction, while the hybrid network's seamline maintains a more regular direction, aligning better with human visual preferences.

In addition to the advantages over other methods, the proposed method still has some limitations. First, in terms of cost map, SGBM does not perform well in vertical overlap, so there is a regression in accuracy performance in Katowice's experiment. Moreover, using only binary cost may ignore many details that need to be bypassed, such as short walls and vehicles. The FGS-based method does better by using a cost map with a mixture of foreground segmentation and NCC result. More critically, the proposed search method works based on points constructed network and edge removing on a binary raster map, so how to apply the hybrid network search method to the more complex and refined cost map to improve the accuracy needs further research.

## V. Conclusion

Optimal seamline search is the core procedure of seamless mosaicking, and its aim is to bypass obvious objects that may create seam effects. In this article, a novel seamline search method based on the hybrid network is presented. It uses a binarized disparity as the cost map, constructs a hybrid network using both edge points and regular grid points simultaneously, and performs an optimal seamline search on the network. Experimental results show that the proposed method can generate high-precision seamlines and has nearly ten times improvement in computational efficiency compared with FGS-based method and OrthoVista. Furthermore, compared to previously fast approach, such as Song's JPS-based method, our method exhibits advantages in terms of efficiency. Moreover, it is more regular in visual effects. Specifically, on Vaihingen's dataset, the proposed method only traversed seven obvious buildings, which is better than the other group. Moreover, the computation took only 47 s, which is more efficient. On the other Katowice dataset, only seven obvious buildings were crossed, and the overall calculation took only 38 s, which is significantly faster than the control method.

Based on the principle of computational time complexity of graph search, the proposed method constructs a hybrid network using both edge points and regular grid points simultaneously. Instead of a raster cost map, the proposed method uses a binarized disparity as the cost map. Therefore, the graph nodes number is significantly reduced, bringing a nearly tenfold improvement in seamline search efficiency.

Compared with the original Voronoi network composed of edge points, the proposed hybrid network construction method can construct a sophisticated network on narrow traversable areas and a regular grid in open areas. Therefore, the proposed method can simultaneously finely bypass dense buildings and maintain a straight line in the good area.

The proposed approach also has some weaknesses; due to the limitation of the disparity map generated by the SGBM algorithm, the proposed method is slightly weaker than the FGS-based method in terms of accuracy, and the binarized cost map construction method is also deficient and may ignore detailed features.

In future work, we will extend the application level of hybrid network search to improve the detection performance of seamlines by introducing a more complex multidimensional cost map. Also, the edge weight of the hybrid network will be further studied to adapt to more complex search situations.

## Acknowledgment

The authors would like to thank the International Society of Photogrammetry and Remote Sensing for providing the benchmark dataset.

## References

[1] Y. Boykov, O. Veksler, and R. Zabih, "Fast approximate energy minimization via graph cuts," *IEEE Trans. Pattern Anal. Mach. Intell.*, vol. 23, no. 11, pp. 1222–1239, Nov. 2001.

[2] M. Kerschner, "Seamline detection in colour orthoimage mosaicking by use of twin snakes," *ISPRS J. Photogramm. Remote Sens.*, vol. 56, no. 1, pp. 53–64, Jun. 2001.

[3] J. Zhang, M. Sun, and Z. Zhang, "Automated seamline detection for orthophoto mosaicking based on ant colony algorithm," *Geomatics Inf. Sci. Wuhan Univ.*, vol. 34, no. 6, pp. 675–678, Jun. 2009.

[4] W.-Y. Lin, S. Liu, Y. Matsushita, T.-T. Ng, and L.-F. Cheong, "Smoothly varying affine stitching," in *Proc. IEEE Conf. Comput. Vis. Pattern Recognit.*, Jun. 2011, pp. 345–352.

[5] E. W. Dijkstra, "A note on two problems in connexion with graphs," *Numerische Math.*, vol. 1, no. 1, pp. 269–271, Dec. 1959.

[6] X. X. Yuan and C. Zhong, "An improvement of minimizing local maximum algorithm on searching seam line tor orthoimage mosaicking," *Acta Geodaetica et Cartographica Sinica*, vol. 41, no. 2, pp. 199–204, Feb. 2012.

[7] L. Li, J. Yao, X. Lu, J. Tu, and J. Shan, "Optimal seamline detection for multiple image mosaicking via graph cuts," *ISPRS J. Photogramm. Remote Sens.*, vol. 113, pp. 1–16, Mar. 2016.

[8] J. Li, Q. Hu, and M. Ai, "Optimal illumination and color consistency for optical remote-sensing image mosaicking," *IEEE Geosci. Remote Sens. Lett.*, vol. 14, no. 11, pp. 1943–1947, Nov. 2017.

[9] J. Li, "Parallax-tolerant image stitching based on robust elastic warping," *IEEE Trans. Multimedia*, vol. 20, no. 7, pp. 1672–1687, Dec. 2017.

[10] L. Li, Y. Li, M. Xia, Y. Li, J. Yao, and B. Wang, "Grid model-based global color correction for multiple image mosaicking," *IEEE Geosci. Remote Sens. Lett.*, vol. 18, no. 11, pp. 2006–2010, Nov. 2021.

[11] L. Li, J. Yao, Y. Liu, W. Yuan, S. Shi, and S. Yuan, "Optimal seamline detection for orthoimage mosaicking by combining deep convolutional neural network and graph cuts," *Remote Sens.*, vol. 9, no. 7, p. 701, Jul. 2017.

[12] L. Li, J. Yao, R. Xie, M. Xia, and W. Zhang, "A unified framework for street-view panorama stitching," *Sensors*, vol. 17, no. 12, p. 1, Dec. 2016.

[13] Q. Wang, G. Zhou, R. Song, Y. Xie, M. Luo, and T. Yue, "Continuous space ant colony algorithm for automatic selection of orthophoto mosaic seamline network," *ISPRS J. Photogramm. Remote Sens.*, vol. 186, pp. 201–217, Apr. 2022.

[14] Y. Wan, D. Wang, J. Xiao, X. Lai, and J. Xu, "Automatic determination of seamlines for aerial image mosaicking based on vector roads alone," *ISPRS J. Photogramm. Remote Sens.*, vol. 76, pp. 1–10, Feb. 2013.

[15] S. Hougardy, "The Floyd–Warshall algorithm on graphs with negative cycles," *Inf. Process. Lett.*, vol. 110, nos. 8–9, pp. 279–281, Apr. 2010.

[16] D. Wang et al., "Using vector building maps to aid in generating seams for low-attitude aerial orthoimage mosaicking: Advantages in avoiding the crossing of buildings," *ISPRS J. Photogramm. Remote Sens.*, vol. 125, pp. 207–224, Mar. 2017.

[17] Q. Chen, M. Sun, X. Hu, and Z. Zhang, "Automatic seamline network generation for urban orthophoto mosaicking with the use of a digital surface model," *Remote Sens.*, vol. 6, no. 12, pp. 12334–12359, Dec. 2014.

[18] M. Zheng, X. Xiong, and J. Zhu, "A novel orthoimage mosaic method using a weighted A algorithm—Implementation and evaluation," *ISPRS J. Photogramm. Remote Sens.*, vol. 138, pp. 30–46, Apr. 2018.

[19] W. Yuan, X. Yuan, Y. Cai, and R. Shibasaki, "Fully automatic DOM generation method based on optical flow field dense image matching," *Geo-Spatial Inf. Sci.*, vol. 26, no. 2, pp. 242–256, Apr. 2023.

[20] W. Yuan, X. X. Yuan, S. Xu, J. Y. Gong, and R. Shibasaki, "Dense image-matching via optical flow field estimation and fast-guided filter refinement," *Remote Sens.*, vol. 11, no. 20, p. 2410, Oct. 2019.

[21] L. Nie, C. Lin, K. Liao, S. Liu, and Y. Zhao, "Unsupervised deep image stitching: Reconstructing stitched features to images," *IEEE Trans. Image Process.*, vol. 30, pp. 6184–6197, 2021.

[22] G. Chen, S. Chen, X. Li, P. Zhou, and Z. Zhou, "Optimal seamline detection for orthoimage mosaicking based on DSM and improved JPS algorithm," *Remote Sens.*, vol. 10, no. 6, p. 821, May 2018.

[23] H.-C. Ma and J. Sun, "Intelligent optimization of seam-line finding for orthophoto mosaicking with LiDAR point clouds," *J. Zhejiang Univ. Sci. C*, vol. 12, no. 5, pp. 417–429, May 2011.
[24] J. Pan, M. Wang, J. Li, S. Yuan, and F. Hu, "Region change rate-driven seamline determination method," *ISPRS J. Photogramm. Remote Sens.*, vol. 105, pp. 141–154, Jul. 2015.
[25] J. Pan, M. Wang, D. Li, and J. Li, "A network-based radiometric equalization approach for digital aerial orthoimages," *IEEE Geosci. Remote Sens. Lett.*, vol. 7, no. 2, pp. 401–405, Apr. 2010.
[26] M. Wang, S. Yuan, J. Pan, L. Fang, Q. Zhou, and G. Yang, "Seamline determination for high resolution orthoimage mosaicking using watershed segmentation," *Photogramm. Eng. Remote Sens.*, vol. 82, no. 2, pp. 121–133, Feb. 2016.
[27] X. X. Yuan, M. M. Duan, and J. S. Cao, "A seam line detection algorithm for orthophoto mosaicking based on disparity image," *Acta Geodaetica et Cartographica Sinica*, vol. 44, no. 8, pp. 877–883, Aug. 2015.
[28] S. Pang, M. Sun, X. Hu, and Z. Zhang, "SGM-based seamline determination for urban orthophoto mosaicking," *ISPRS J. Photogramm. Remote Sens.*, vol. 112, pp. 1–12, Feb. 2016.
[29] H. Hirschmuller, "Stereo processing by semiglobal matching and mutual information," *IEEE Trans. Pattern Anal. Mach. Intell.*, vol. 30, no. 2, pp. 328–341, Feb. 2008.
[30] X. Li, R. Feng, X. Guan, H. Shen, and L. Zhang, "Remote sensing image mosaicking: Achievements and challenges," *IEEE Geosci. Remote Sens. Mag.*, vol. 7, no. 4, pp. 8–22, Dec. 2019.
[31] S. Yuan, K. Yang, X. Li, and H. Cai, "Automatic seamline determination for urban image mosaicking based on road probability map from the D-LinkNet neural network," *Sensors*, vol. 20, no. 7, p. 1832, Mar. 2020.
[32] Q. Dai, F. Fang, J. Li, G. Zhang, and A. Zhou, "Edge-guided composition network for image stitching," *Pattern Recognit.*, vol. 118, Oct. 2021, Art. no. 108019.
[33] L. Li, J. Tu, Y. Gong, J. Yao, and J. Li, "Seamline network generation based on foreground segmentation for orthoimage mosaicking," *ISPRS J. Photogramm. Remote Sens.*, vol. 148, pp. 41–53, Feb. 2019.
[34] M. Song et al., "Mosaicking UAV orthoimages using bounded Voronoi diagrams and watersheds," *Int. J. Remote Sens.*, vol. 39, nos. 15–16, pp. 4960–4979, 2018.

**Wei Yuan** (Member, IEEE) received the M.E. and Ph.D. degrees from The University of Tokyo, Tokyo, Japan, in 2015 and 2018, respectively.

He joined the Center for Spatial Information Science, The University of Tokyo, as a Researcher, 2018, where he became an Assistant Professor in 2020. He is currently an Associate Professor with the International Research Institute of Disaster Science, Tohoku University, Sendai, Japan. His research interests include photogrammetry, remote sensing, GIS, and computer vision, especially in image matching, 3-D reconstruction, and change detection.

**Yang Cai** received the bachelor's, master's, and Ph.D. degrees from the School of Remote Sensing and Information Engineering, Wuhan University, Wuhan, China, in 2013, 2016, and 2023, respectively.

He is currently with Changjiang Space Information Technology Engineering Company Ltd., Wuhan, where he specializes in remote sensing and photogrammetry. His research interests include photogrammetry, computer vision, and related fields.

**Jonathan Li** (Fellow, IEEE) received the Ph.D. degree in geomatics engineering from the University of Cape Town, Cape Town, South Africa, in 2000.

He is currently a Professor of geomatics and systems design engineering with the University of Waterloo, Waterloo, ON, Canada. He has coauthored over 600 publications, more than 150 of which were published in top remote sensing journals, including *Remote Sensing of Environment*, *ISPRS Journal of Photogrammetry and Remote Sensing*, IEEE TRANSACTIONS ON GEOSCIENCE AND REMOTE SENSING, and *International Journal of Applied Earth Observation and Geoinformation* (JAG). He has also published papers in flagship conferences in computer vision and AI, including CVPR, AAAI, and IJCAI. He has supervised nearly 200 master's/Ph.D. students as well as post-doctoral fellows/visiting scholars to completion. His main research interests include AI-based information extraction from Earth observation images and LiDAR point clouds, pointgrammetry and remote sensing, GeoAI and 3-D vision for digital twin cities, and autonomous driving.

Dr. Li is a fellow of the Canadian Academy of Engineering, the Royal Society of Canada (Academy of Science), and the Engineering Institute of Canada. He is the President of the Canadian Institute of Geomatics (CIG). He is the Editor-in-Chief of JAG and an Associate Editor of the IEEE TRANSACTIONS ON GEOSCIENCE AND REMOTE SENSING and IEEE TRANSACTIONS ON INTELLIGENT TRANSPORTATION SYSTEMS.